Eur. Phys. J. D **20**, 227–232 (2002)
DOI: 10.1140/epjd/e2002-00124-1

THE EUROPEAN PHYSICAL JOURNAL D

Application of the stabilization method to interacting resonances

T. González-Lezana[1], G. Delgado-Barrio[2], P. Villarreal[2,a], and F.X. Gadéa[3]

[1] Physical and Theoretical Chemistry Laboratory, South Parks Road, Oxford OX1 3QZ, UK
[2] Instituto de Matemáticas y Física Fundamental (CSIC) Serrano 123, 28004 Madrid, Spain
[3] Laboratoire de Physique Quantique, Université Paul Sabatier, 118 route de Narbonne, 31062 Toulouse Cedex 04, France

Received 5 April 2002 / Received in final form 24 May 2002
Published online 19 July 2002 –

Abstract. The stabilization method is applied to the case of interacting resonances in the photo-dissociation of van der Waals clusters composed by a rare gas atom bound to a dihalogen molecule. The study of an illustrative two-dimensional model consisting in a T-shaped NeI_2 molecule shows the adequacy of the method whenever the projection of the stabilization wave functions on the assumed prepared initial state is accounted for. The agreement of the fragmentation cross-sections with some previous results using the effective resolvent method and accurate close-coupling calculations is excellent. The method reveals its utility as a complementary tool since allows, through the analysis of the stabilization wave function in terms of zero-order levels, a precise characterization of the resonant states involved.

PACS. 33.40.+f Multiple resonances (including double and higher-order resonance processes, such as double nuclear magnetic resonance, electron double resonance, and microwave optical double resonance) – 33.80.Gj Diffuse spectra; predissociation, photodissociation – 34.30.+h Intramolecular energy transfer; intramolecular dynamics; dynamics of van der Waals molecules

1 Introduction

Resonant phenomena, where an excited quasi-bound state is formed for a finite lapse of time to finally decay as a consequence of the coupling with different continua, is commonplace in many fields of physics. Special interest has been devoted to those situations where it is possible to find quantum-interference effects between resonances [1]. One particular example is the photo-fragmentation of van der Waals (vdW) clusters $X\cdots Y_2$ formed by a rare gas atom (X) and a dihalogen molecule (Y_2). In this process, the diatomic partner is promoted by means of a photon excitation to a both electronically and vibrationally excited state within the complex, $XY_2^*(v_0)$, which in turn fragmentates as a result of the energy transfer from the diatomic vibrational mode to the vdW stretching mode. This constitutes the mechanism of vibrational predissociation (VP). In the simplest case, the process may proceed *via* direct coupling between the initially excited state of the complex and the different dissociative continua. The absorption cross-sections obtained in this case present a Lorentzian profile typically associated to isolated resonances. For the $HeBr_2$ complex, for instance, it was found that the direct mechanism uses to be the main photo-fragmentation pathway when the bromine is excited to vibrational states with $v_0 \leq 38$ in the B electronic state [2]. As soon as higher vibrational states, close to the dissociation limit ($v_0 \geq 42$), are initially excited an intramolecular vibrational-energy redistribution (IVR) mechanism involving the energy flowing from the halogen vibration to vdW excited modes of lower vibrational manifolds ($v < v_0$) competes with VP [3,4]. This scenario thus involves the presence of additional resonant quasi-bound states, energetically close to that initially promoted by the photon excitation, which are populated before the fragmentation process takes place. The coupling among these quasi-bound states produces complicated cross-section profiles which reveals the presence of interacting resonances. Similar features of an IVR mechanism have been found in the fragmentation dynamics of several vdW complexes such as ArI_2[5], $ArCl_2$[6,7], NeI_2 [8] and $NeBr_2$ [9].

We have recently extended the effective resolvent method, based on the wave operator theory of quantum dynamics [10], to the case of interacting resonances [11]. In that work where a T-shaped NeI_2 vdW cluster was studied, the presence of two zero-order states (ZOS) nearly degenerated ($|v = 35, n = 0\rangle$ and $|34, 4\rangle$, where v denotes the I_2 vibrational level while n is the quantum number associated to the Ne–I_2 stretching motion) creates the two interacting resonances scenario studied there [11]. The effective resolvent results were compared with time-dependent wave-packet propagations and with accurate close-coupling calculations in the energy domain, probing its numerical efficiency.

[a] e-mail: p.villarreal@imaff.cfmac.csic.es

In this work, we complete our previous study on NeI_2 [11] by applying the stabilization method [12,13]. This technique has been successfully used to characterize resonances and to obtain probability distributions in a number of dynamical processes [14–16]. The procedure followed here is closely related to that previously applied to the $HeBr_2$ complex [3] in which for the first time, in order to obtain accurate cross-section profiles of fragmentation, not only the variation of the energy with a stabilization parameter but also the projection of the stabilization wave function on the prepared initial state is taken into account. In addition, and as in reference [11], we consider here four different initial states: the two zero-order levels mentioned above, $|35,0\rangle$ and $|34,4\rangle$, together with two extreme linear combinations of them, $(1/\sqrt{2})(|35,0\rangle+|34,4\rangle)$ and $(1/\sqrt{2})(|35,0\rangle-|34,4\rangle)$, which almost diagonalize the Hamiltonian in the discrete subspace. In this way, the relevance of including such initial states through projections of the stabilization wave function, in order to estimate cross-section profiles, is shown. Furthermore, the analysis of the stabilization wave function allows to characterize the resonant states involved in the fragmentation process.

The goal of this study is to illustrate how such a simple method, in comparison with some other conventional treatments that required much more work, can provide however extremely helpful information. In the particular case treated here the method, despite its great simplicity, offers a detailed and precise insight of the physics of the interacting resonances.

The basic theory which underlies the method is briefly described in Section 2, while the results are presented and discussed in Section 3. Finally, Section 4 collects the conclusions of this work.

2 Theory

The Hamiltonian for the T-shaped triatomic system in Jacobi coordinates can be written as follows:

$$H = \frac{-\hbar^2}{2\mu_2}\frac{\partial^2}{\partial r^2} + V(r) - \frac{\hbar^2}{2\mu_3}\frac{\partial^2}{\partial R^2} + W(R,r,\theta=\pi/2), \tag{2.1}$$

where r is the elongation of the diatomic molecule I_2, $V(r)$ its potential for the B electronic state and μ_2 the corresponding reduced mass. In turn, R is the distance from the diatomic center of mass to the Ne atom, with μ_3 being the Ne–I_2 reduced mass, and W is the intermolecular potential described as an addition of pairwise interactions [17]. Finally θ is the angle formed by the vectors r and R.

The eigenfunctions of the Hamiltonian in equation (2.1) are expanded as follows:

$$\Phi_m(R,r;\alpha) = \sum_{vj} a_{vj}^m(\alpha)\chi_v(r)\phi_j(R;\alpha) \tag{2.2}$$

where $\chi_v(r)$ are the eigenstates of the diatomic I_2(B) system. For the R coordinate a discrete variable representation (DVR) scheme based on particle-in-a-box (PINAB) eigenfunctions is adopted. Following reference [18], the $\phi_j(R;\alpha)$ functions in (2.2) are given by:

$$\phi_j(R;\alpha) = \frac{2}{\sqrt{L_\alpha(N+1)}}\sum_{k=1}^{N}\sin\frac{k\pi(R-R_0)}{L_\alpha}\sin\frac{k\pi j}{N+1}, \tag{2.3}$$

with N being the size of this basis set considered in the calculation and $L_\alpha = R_{\max}(\alpha) - R_0$ the length of the box. Such basis functions depend on an α parameter through the upper limit as follows:

$$R_{\max}(\alpha) = R_{\max}^{(0)} - \alpha, \tag{2.4}$$

where $R_{\max}^{(0)}$ is some initial guess for such a value. Discrete values for the coordinate R within this DVR formalism are finally given by:

$$R_{j\alpha} = \frac{jL_\alpha}{N+1} + R_0,\ j = 1,...,N. \tag{2.5}$$

The stabilization method consists basically in carrying out successive diagonalizations of the Hamiltonian matrix using slightly different basis sets which depend on the α parameter. By varying the value of α it is possible to identify quasi-bound states or resonances of the system from the stable behavior (in terms of α) of their corresponding energies. The $\mathcal{L}^2$ representations of purely continuum functions assumed by the method will however strongly depend on α and not present a quasi-vertical character in a stabilization diagram where α is plotted *versus* the energy.

For each value of α, by diagonalizing the Hamiltonian, stabilization wave functions $\Phi_m(\alpha)$ and corresponding energies $E_m(\alpha)$ are obtained. Within this formalism, the discrete, stick form of cross-section averaged over a $\Delta\alpha$ range for the fragmentation of the system initially prepared in a particular $|vn\rangle$ ZOS in the excited electronic B state, can be written, in a similar way to that of reference [3]:

$$\langle\sigma_{vn}(E)\rangle \sim (\Delta\alpha)^{-1}\sum_m \left|\frac{\mathrm{d}E_m}{\mathrm{d}\alpha}\right|^{-1}_{\alpha_m^*} w_{vn}^{(m)}(\alpha_m^*). \tag{2.6}$$

In this equation the right hand expression refers to the averaged spectral density or density of states after such a fragmentation process, $\langle\rho_{vn}(E)\rangle$, calculated by means of the stabilization method, and $w_{vn}^{(m)}(\alpha_m^*)$ is the weight of the stabilization wave-function on the $|vn\rangle$ ZOS, for the α parameter value at which $E_m(\alpha_m^*) = E$, that is

$$w_{vn}^{(m)}(\alpha) = |\langle\Phi_m(\alpha)\mid\psi_{vn}(\alpha)\rangle|^2. \tag{2.7}$$

In turn, the $\psi_{vn}(\alpha)$ functions in equation (2.7) for these ZOS's are obtained as the eigenstates of the Hamiltonian of equation (2.1) for a given vibrational v state, $\langle v|H|v\rangle$, and can be expressed as:

$$\psi_{vn}(R,r;\alpha) = \chi_v(r)\sum_j b_j^{(vn)}\phi_j(R;\alpha). \tag{2.8}$$

Dealing with interacting resonances it is interesting to also consider some linear combinations of the coupled ZOS's. Thus, since the states mainly involved in this particular case under study, $|35,0\rangle$ and $|34,4\rangle$, become nearly degenerated as will be shown below, the following combinations were additionally taken into account in our calculations:

$$\psi_{\pm} = \frac{1}{\sqrt{2}} \left(\psi_{35,0} \pm \psi_{34,4} \right). \tag{2.9}$$

Obviously, the overlap between such $\psi_{\pm}$ functions and the stabilization wave-function can be expressed in terms of those defined in equation (2.7) as follows:

$$w_{\pm}^{(m)} = \frac{1}{2} \left(w_{35,0}^{(m)} + w_{34,4}^{(m)} \pm 2 \langle \Phi_m \mid \psi_{35,0} \rangle \langle \Phi_m \mid \psi_{34,4} \rangle \right). \tag{2.10}$$

Such a definition requires, in order to distinguish between contributions to $w_{+}^{(m)}$ and those to $w_{-}^{(m)}$, that the numerical phase of functions ψ_{vn} is consistently defined. Therefore, in order to ensure so, we force those functions to adopt a positive value for the last DVR point R_N. Thus, from equation (2.8), the following condition:

$$\sum_j b_j^{(vn)} \phi_j(R_N;\alpha) > 0 \tag{2.11}$$

must be satisfied by the ZOS wave-functions.

The study of the interacting resonances found for the system treated in this work is finally completed with the probability densities for those energies of interest. These densities are easily obtained from the stabilization wave-function for a particular value of α as:

$$\mathcal{D}_m(R,r;\alpha) = \mid \Phi_m(R,r;\alpha) \mid^2 . \tag{2.12}$$

3 Results

In the calculations, five eigenstates $\chi_v(r)$ of the diatomic I_2 system from $v = 32$ up to $v = 36$ were employed. The potential for the I–I interaction was taken from reference [19] Those functions were defined in a grid of 500 Gauss-Legendre points between $r = 2.6$ Å and $r = 4.7$ Å. For the R coordinate 250 DVR points were used from the same number of PINAB functions. Initially the box where those points were defined was set between 1.5 Å and 25 Å with the upper limit decreasing successively in steps of 0.005 Å. The stabilization diagrams were computed for α values in the range [0−3.035] Å.

3.1 Stabilization diagram and densities of states

From Figure 1, where the level structure for $v = 34$ and $v = 35$ vibrational manifolds is shown, it is clear that $|35,0\rangle$ and $|34,4\rangle$ ZOS's may become coupled since their corresponding energies are almost degenerate ($E_{35,0} = -67.98$ cm^{-1}, $E_{34,4} = -68.42$ cm^{-1}). In order to analyze the consequences of such a coupling between these

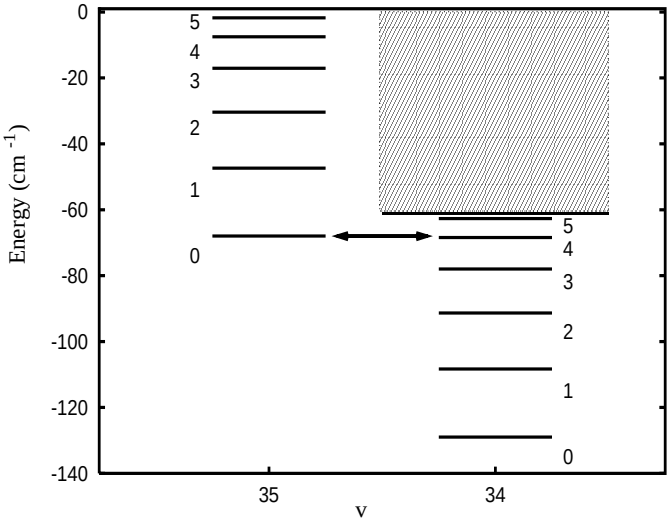

Fig. 1. Quasi-bound states and continua of the T-shaped NeI_2(B) system for $v = 34, 35$ diatomic vibrational states. For each vibrational manifold, vdW modes are labelled from 0 up to 5. Energies are referred to the $E_{I_2}(v = 35)$ diatomic level.

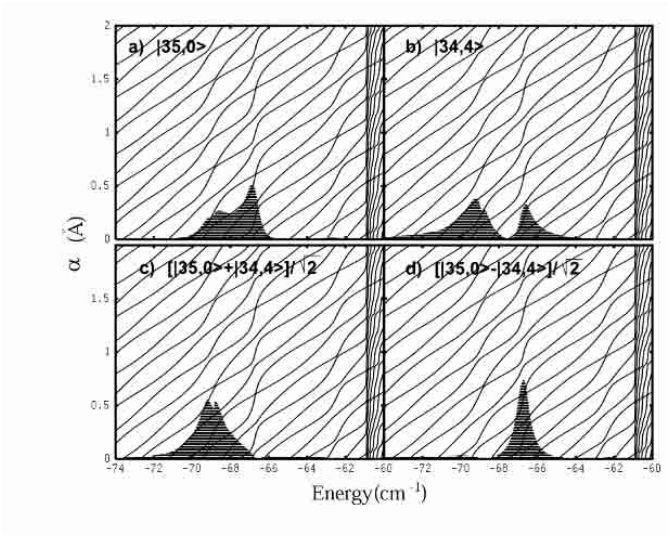

Fig. 2. Stabilization diagram: variation of the α parameter *versus* the energy showing, as quasi-vertical lines, the regions at which some resonance could appear. Dominant weights at each energy, $\max\{w_{vn}^{(m)}\}$ and $\max\{w_{\pm}^{(m)}\}$, defined after equations (2.7, 2.10) respectively, are also depicted as shadow lines. In panel (a) results for $w_{35,0}^{(m)}$, in (b) for $w_{34,4}^{(m)}$ and panels (c) and (d) are for $w_{+}^{(m)}$ and $w_{-}^{(m)}$ respectively.

two states, stabilization calculations were performed to simulate fragmentations from those ZOS's and from their linear combinations defined in equation (2.9). The stabilization diagram where the α parameter is plotted *versus* the energy is shown in all the panels in Figure 2. In panel (a), the dominant weight at each energy, for the initial state $|35,0\rangle$, $\max\{w_{35,0}^{(m)}\}$, is also depicted. The corresponding dimensionless values vary obviously within the interval $[0,1]$, and to simplify the plot we have used the

same ordinate scale than for the α parameter. Similarly, panels (b) through (d) collect the corresponding dominant weights for an initial state $|34,4\rangle$ and the above mentioned linear combinations, respectively besides the same stabilization diagram. The diagram reveals the onset of the diatomic vibrational ($v = 34$)-manifold around -61 cm^{-1}, clearly unaffected by the variations in the streching coordinate R, and three different regions with a stable behavior. In particular, the logical surmise which would relate stability found around -69 and -67 cm^{-1} (which we will denote as $\mathcal{L}$ and $\mathcal{R}$, respectively) with the interacting ZOS's mentioned before is confirmed by the profiles resulting from the overlaps $\max\{w^{(m)}_{35,0}\}$ and $\max\{w^{(m)}_{34,4}\}$ (panels (a) and (b) respectively). The coupling between the two states yields intense peaks around both energies regardless of the precise $|vn\rangle$ state considered in equation (2.7). This is the result found in those systems where one particular state displays optical activity absorbing the photon excitation and playing thus the role of a "bright" state, while some other "dark" states, energetically coupled to the former, turn to be also activated by means of an IVR mechanism [3,7]. On the contrary, a similar calculation not shown here for the $|34,5\rangle$ ZOS as the initial state reveals that it is almost decoupled from the rest. In fact, a single maximum peak appears clearly centered around the stable region found near -62 cm^{-1}, which is the expected behavior for isolated resonances.

In addition, it is worth mentioning that the results of the calculations performed using weights $w^{(m)}_{\pm}$, shown in Figures 2c and 2d, demonstrate that ψ_+ and ψ_- functions are correlated with the stable behavior found around $\mathcal{L}$ and $\mathcal{R}$ energies.

From the weights and the information contained in the stabilization diagram commented above it is possible to extract the spectral densities and thus the corresponding cross-sections for the fragmentation process under study using equation (2.6). In Figures 3a–3d we show in arbitrary units $\langle\rho_{35,0}(E)\rangle$, $\langle\rho_{34,4}(E)\rangle$, $\langle\rho_+(E)\rangle$, and $\langle\rho_-(E)\rangle$ densities of states, respectively. In these figures, stabilization results are compared with those obtained by means of the effective resolvent method and accurate close-coupling calculations reported in reference [11]. The agreement found among the three different methods is excellent, giving confidence in these various approaches. There is a direct relationship between the width of the peaks in the density of state profile and the slope of the curves $\alpha(E)$ in the stabilization diagram, in the sense that narrow peaks are the result of more vertical (that is more stable) curves which correspond to resonances with very well defined values of energy. In this sense the peak found for the $\mathcal{R}$ resonance becomes more intense and narrower than that for the $\mathcal{L}$ resonance.

Furthermore, the quasi-Lorentzian profiles shown in panels (c) and (d) are consequence of the fact that the considered linear combinations of two ZOS's are close to eigenstates of the discrete part of the Hamiltonian and turn to be suitable choices to describe the quasi-bound states as isolated resonances. Necessity of accounting for both ZOS's, in order to describe correctly the fragmentation dynamics in the energy range studied here, is therefore just a natural consequence of the existence of an interacting-resonances scenario.

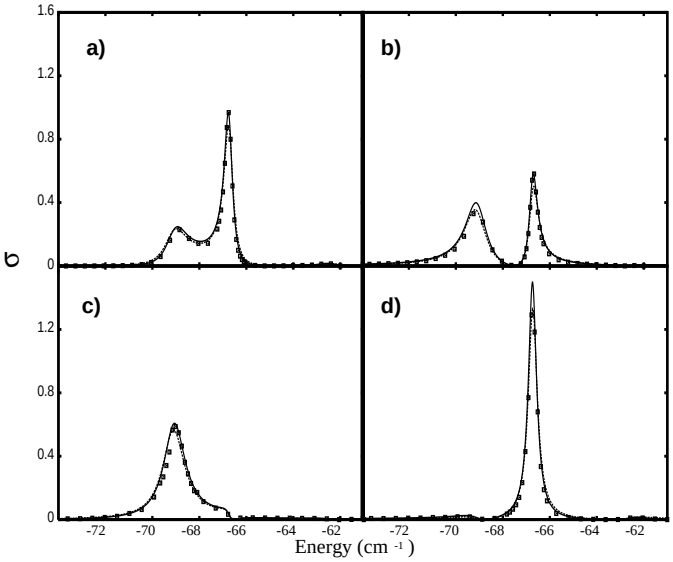

Fig. 3. Averaged densities of states calculated with the stabilization method (points) as defined in equation (2.6) for the photo-fragmentation of the T-shaped $NeI_2(B)$ cluster when the system is initially prepared in the following ZOS's: (a) $|35,0\rangle$, (b) $|34,4\rangle$, and the linear combinations (c) $[|35,0\rangle + |34,4\rangle]/\sqrt{2}$ and (d) $[|35,0\rangle - |34,4\rangle]/\sqrt{2}$. With lines, close-coupling (solid) and effective resolvent (dashed) calculations from reference [11].

3.2 Probability densities

One of the most useful features of the stabilization method when studying resonant states is the possibility of obtaining the wave-function associated to the quasi-bound states found in the calculation. In order to analyze the structure of the resonant wave-functions, Figure 4 displays the distributions corresponding to the two ZOS's mainly involved. From the probability density $\mathcal{D}_m(R,r;\alpha)$ defined in equation (2.12) and calculated at those particular values of the α parameter where a stable behavior is observed, an analysis of the relevant wave-function can be carried out. To characterize the two interacting resonant states, probability densities were calculated at $\alpha = 2.520$ Å for the $\mathcal{L}$ resonance and $\alpha = 1.285$ Å in the case of the $\mathcal{R}$ resonance. The densities obtained for such values in both cases are shown in Figures 5a and 6a respectively. The components of the corresponding resonant wave-functions on the different I_2 vibrational manifolds and the weights on the ZOS's of interest are presented in Table 1. The $\mathcal{L}$ and $\mathcal{R}$ resonances are located at -69.20 cm^{-1} and -66.84 cm^{-1} respectively. Owing to the proper choice of the α parameters, these eigenvalues associated to the two resonances should not differ too much from those obtained fitting the stabilization cross-sections to analytical expressions [1,20,21].

Table 1. Analysis of the resonant states ($\mathcal{L}$ and $\mathcal{R}$) from the associated wave-function. In the second column, order m of the eigenstate in the diagonalization performed at the corresponding value of the α parameter given in the third column. In the fourth column, energy E of the resonant state. From fifth up to eighth column, total weights in each vibrational manifold, the last two columns collecting the weights in $|35,0\rangle$ and $|34,4\rangle$ ZOS's, respectively.

Res	m	α(Å)	E(cm^{-1})	$w_{32}^{(m)}$	$w_{33}^{(m)}$	$w_{34}^{(m)}$	$w_{35}^{(m)}$	$w_{35,0}^{(m)}$	$w_{34,4}^{(m)}$
$\mathcal{L}$	175	2.520	−69.198	0.160	0.234	0.402	0.204	0.195	0.386
$\mathcal{R}$	256	1.285	−66.836	0.027	0.221	0.243	0.509	0.501	0.208

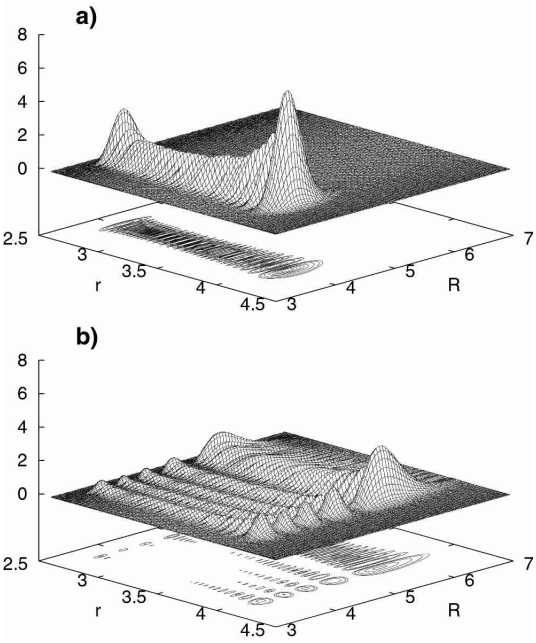

Fig. 4. Probability densities of the ZOS's at $\alpha = 2.52$ Å: (a) $|\psi_{35,0}|^2$ and (b) $|\psi_{34,4}|^2$. Distances r and R in Å.

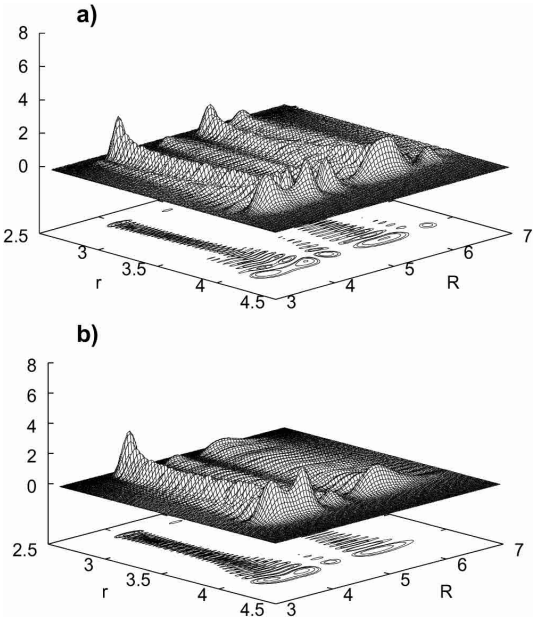

Fig. 5. (a) $\mathcal{D}_m(R,r)$ probability density as defined in equation (2.12) for $\mathcal{L}$ resonance at $\alpha = 2.52$ Å, and (b) probability density for the ψ_+ linear combination.

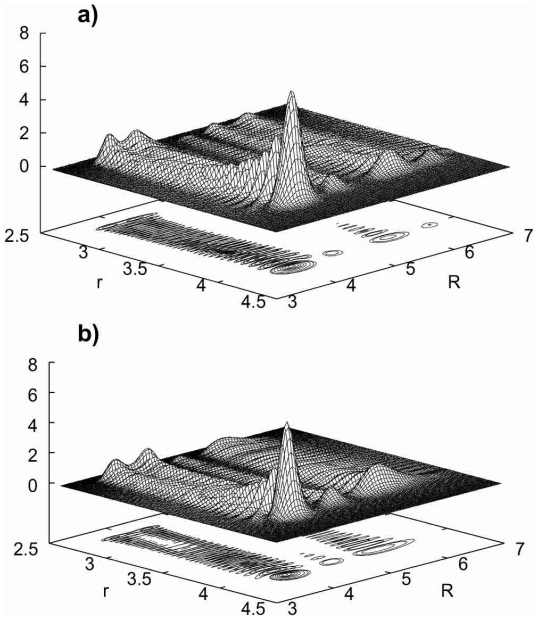

Fig. 6. Same as Figure 5 for (a) $\mathcal{R}$ resonance at $\alpha = 1.285$ Å and (b) for ψ_-.

From Figures 5a and 6a it is easy to observe the consequences of the interaction of the two ZOS's involved in the resonant process. In both cases the 2D probability density $\mathcal{D}_m(R,r)$ shows features of four quasi-nodes in the R-direction, specially for the $\mathcal{L}$ resonance, Figure 5a, in the region of [4−4.5] Å for r, as expected since the $|34,4\rangle$ ZOS is playing a significant role. Analogously, the strong maximum found for the $\mathcal{R}$ resonance, Figure 6a, at $r \sim 4.2$ Å and $R \sim 4$ Å reveals the presence of the $|35,0\rangle$ ZOS. These indications are clearly corroborated by the values of weights $w_{35,0}^{(m)}$ and $w_{34,4}^{(m)}$ shown in Table 1: in $\mathcal{L}$ resonance we find a mixture of about 20% of the $|35,0\rangle$ state and about 39% of $|34,4\rangle$ state, whereas $\mathcal{R}$ resonance turns to be the result of a 50% and 21% of $|35,0\rangle$ and $|34,4\rangle$ ZOS's respectively. Moreover, these two ZOS's are responsible of the total component of the ($v = 35$)- and ($v = 34$)-manifolds in both resonances, suggesting that the participation of some other possible $|35, n \neq 0\rangle$ and $|34, n \neq 4\rangle$ ZOS's is almost negligible. Considerable contribution from the the two other lower vibrational manifolds $v < 34$ is also obtained but it is originated exclusively by ($v = 33$)- and ($v = 32$)-continua since no ZOS's such that $E_{vn} < E_{I_2}(v)$ exist in the energy range studied here for any of those vibrational states.

The resonant states cannot be identified with individual ZOS, as can be seen comparing Figure 4 with Figures 5a and 6a. On the contrary, and to stress the fact that the linear combinations of the two ZOS's already mentioned closely represent the resonance states corresponding to $\mathcal{L}$ and $\mathcal{R}$, we display in Figures 5b and 6b the 2D distributions $|\psi_+|^2$ and $|\psi_-|^2$, respectively. One clearly sees the similarities of panels (a) and (b) within each of the Figures 5 and 6, in particular for R values lower than 5 Å; at longer distances, contributions from the continua become more significant and give rise to stronger differences between each actual resonant state and the corresponding purely discrete linear combination.

Finally, and as was mentioned above, by inspecting the weight $w^{(m)}_{34,5}$ and carrying out a similar analysis for $\alpha = 0.935$ Å, one sees that the corresponding resonant state for the stable curves found at $E \sim -62$ cm^{-1} has a component on the $(v = 35)$-manifold only of $\sim 2\%$, while the presence of the $(v = 34)$-manifold grows up to $\sim 64\%$ due exclusively to the $|34, 5\rangle$ ZOS. No interaction with some other ZOS's then takes place at this energy region.

4 Conclusions

Application of the stabilization method to a case of interacting resonances in the fragmentation process of a T-shaped $NeI_2(B)$ complex illustrates the feasibility and suitability of the method to deal with such interesting phenomena. The extreme simplicity of the procedure (only diagonalizations of the Hamiltonian matrix are required) contrasts with the detailed and complete information that is possible to obtain.

Resonances are identified by means of the stable behavior of the energy curves in the stabilization diagram, and the overlap of the assumed initially prepared state with the corresponding stabilization wave-function is employed to calculate fragmentation densities of states. Comparison with results obtained by using some other methods give us confidence on the accuracy of the stabilization procedure. Moreover, analysis of the probability density functions corresponding to the resonant states clarify the composition of such resonances and the role played by the $|v, n\rangle$ ZOS's required to explain the interaction effects.

This work was supported by the joint CSIC-CNRS project 2000FR0029 and the DGICYT Spanish Grant No. BCM2001-2179. TG-L is indebted to TMR European network, Grant No. HPRN-CT-1999-00007. We thank Philippe Durand for many fruitful discussions.

References

1. For a recent example see B.R. Lewis, S.T. Gibson, P. O'Keeffe, T. Ridley, K.P. Lawley, R.J. Donovan, Phys. Rev. Lett. **86**, 1478 (2001), references therein
2. T. González-Lezana, M.I. Hernández, G. Delgado-Barrio, A.A. Buchachenko, P. Villarreal, J. Chem. Phys. **105**, 7454 (1996)
3. T. González-Lezana, M.I. Hernández, G. Delgado-Barrio, P. Villarreal, J. Chem. Phys. **106**, 3216 (1997)
4. A. Rohrbacher, T. Ruchti, K.C. Janda, A.A. Buchachenko, M.I. Hernández, T. González-Lezana, P. Villarreal, G. Delgado-Barrio, J. Chem. Phys. **110**, 256 (1999)
5. S.K. Gray, O. Roncero, J. Phys. Chem. **99**, 2512 (1995); O. Roncero, S.K. Gray, J. Chem. Phys. **104**, 4999 (1996)
6. D.D. Evard, C.R. Bieler, J.I. Cline, N. Sivakumar, K.C. Janda, J. Chem. Phys. **89**, 2829 (1988)
7. N. Halberstadt, J.A. Beswick, O. Roncero, K.C. Janda, J. Chem. Phys. **96**, 2404 (1992); N. Halberstadt, S. Serna, O. Roncero, K.C. Janda, J. Chem. Phys. **97**, 341 (1992); O. Roncero, D. Caloto, K.C. Janda, N. Halberstadt, J. Chem. Phys. **107**, 1406 (1997) and references by the same authors therein
8. O. Roncero, J. Campos-Martínez, A.M. Cortina, P. Villarreal, G. Delgado-Barrio, Chem. Phys. Lett. **148**, 62 (1988)
9. T.A. Stephenson, N. Halberstadt, J. Chem. Phys. **112**, 2265 (2000); O. Roncero, J. Campos-Martinez, M.I. Hernandez, G. Delgado-Barrio, P. Villarreal, J. Rubayo-Soneira, J. Chem. Phys. **115**, 2566 (2001)
10. Ph. Durand, J.P. Malrieu, in *Ab initio Methods in Quantum Chemistry I*, edited by K.P. Lawley (Wiley, New York, 1987), p. 59; Ph. Durand, I. Paidarová, Phys. Rev. A **58**, 1867 (1998); Ph. Durand, F.X. Gadéa, I. Paidarová, Phys. Chem. Chem. Phys. **2**, 2829 (2000)
11. F.X. Gadéa, Ph. Durand, T. González-Lezana, G. Delgado-Barrio, P. Villareal, Eur. Phys. J. D **15**, 215 (2001)
12. See for example, H.S. Taylor, G.V. Nazaroff, A. Golebieswki, J. Chem. Phys. **45**, 2872 (1966); H.S. Taylor, Adv. Chem. Phys. **18**, 91 (1970); V.A. Mandelshtam, T.R. Ravuri, H.S. Taylor, Phys. Rev. Lett. **70**, 1932 (1993)
13. V.A. Mandelshtam, T.R. Ravuri, H.S. Taylor, Phys. Rev. A **48**, 818 (1993)
14. M.I. Hernández, D.C. Clary, J. Chem. Phys. **101**, 2779 (1994)
15. T. González-Lezana, D.E. Manolopoulos, Farad. Discuss. **110**, 213 (1998)
16. T. Takayanagi, A. Wada, Chem. Phys. Lett. **348**, 514 (2001)
17. A. García-Vela, J. Rubayo-Soneira, G. Delgado-Barrio, P. Villarreal, J. Chem. Phys. **104**, 8405 (1996)
18. J.T. Muckerman, Chem. Phys. Lett. **173**, 200 (1990)
19. M. Groebele, A.H. Zewail, J. Chem. Phys. **98**, 883 (1993)
20. U. Fano, Phys. Rev. **124**, 1866 (1961)
21. F.H. Mies, Phys. Rev. **175**, 164 (1968)